Received: 30 March 2022 | Revised: 6 August 2022 | Accepted: 17 August 2022

DOI: 10.1002/jmor.21508

RESEARCH ARTICLE

JOURNAL OF morphology WILEY

Intraspecific variation in the cranial osteology of *Diplometopon zarudnyi* (Squamata: Amphisbaenia: Trogonophidae)

Rebecca K. Hawkins[1] | **Christopher J. Bell**[2] | **Jennifer C. Olori**[3] | **Michelle R. Stocker**[4]

[1]Department of Fish and Wildlife Conservation, Virginia Tech, Blacksburg, Virginia, USA

[2]Department of Geological Sciences, The University of Texas at Austin, Austin, Texas, USA

[3]Biological Sciences Department, State University of New York at Oswego, Oswego, New York, USA

[4]Department of Geosciences, Virginia Tech, Blacksburg, Virginia, USA

Correspondence
Rebecca K. Hawkins, University of Kansas, Lawrence, KS, USA
Email: rebecca.hawkins@ku.edu

Present address
Rebecca K. Hawkins, Museum Studies Program, Lippincott Hall Room 6, 1410 Jayhawk BlvdLawrence, Kansas, USA.

Funding information
National Science Foundation, Grant/Award Number: 1655609

Abstract

A snake-like body plan and burrowing lifestyle characterize numerous vertebrate groups as a result of convergent evolution. One such group is the amphisbaenians, a clade of limbless, fossorial lizards that exhibit head-first burrowing behavior. Correlated with this behavior, amphisbaenian skulls are more rigid and coossified than those of nonburrowing lizards. However, due to their lifestyle, there are many gaps in our understanding of amphisbaenian anatomy, including how their cranial osteology varies among individuals of the same species and what that reveals about constraints on the skull morphology of head-first burrowing taxa. We investigated intraspecific variation in the cranial osteology of amphisbaenians using seven individuals of the trogonophid *Diplometopon zarudnyi*. Variation in both skull and individual skull element morphology was examined qualitatively and quantitatively through three-dimensional (3D) models created from microcomputed tomography data. Qualitative examination revealed differences in the number and position of foramina, the interdigitation between the frontals and parietal, and the extent of coossification among the occipital complex, fused basioccipital and parabasisphenoid ("parabasisphenoid-basioccipital complex"), and elements X. We performed 3D landmark-based geometric morphometrics for the quantitative assessment, revealing shape differences in the skull, premaxilla, maxilla, frontal, and parietal. The observed intraspecific variation may be the result of different stages of ontogenetic development or biomechanical optimization for head-first burrowing. For example, variation in the coossification of the occipital region suggests a potential ontogenetic coossification sequence. Examination of these areas of variation across other head-first burrowing taxa will help determine if the variation is clade-specific or part of a broader macroevolutionary pattern of head-first burrowing.

KEYWORDS
computed tomography, fossorial, geometric morphometrics, head-first burrowing, skull morphology

1 | INTRODUCTION

A fossorial ecology favors a specialized suite of adaptations, such as a snake-like body plan and a burrowing technique directed by the head, known as head-first burrowing (HFB). Through convergent evolution those adaptions appeared across Vertebrata, with representatives among fish (e.g., Herrel et al., 2011), caecilians (e.g., Sherratt et al., 2014), and many groups of squamates (e.g., Gans, 1974; Lee, 1998). Although snakes may be the most recognizable taxa with this body plan, not all are fossorial today (see Da Silva et al., 2018 for the possible fossorial ancestry of snakes).

Another fossorial squamate group is Amphisbaenia, a clade of approximately 200 species, all but three of which are limbless (Gans, 2005). Amphisbaenians inhabit tropical and subtropical areas in North America, South America, Africa, and Europe (Longrich et al., 2015), where they use their burrowing ability to prey on invertebrates and other small vertebrates. Because of their fossorial ecology and the scarcity of captive individuals (Goetz, 2007), amphisbaenians are elusive and not well-studied. However, their unusual skull morphology has long generated research interest in their osteology.

The rigid and coossified skulls of amphisbaenians are hypothesized to be correlated with their HFB behavior. Within Amphisbaenia there are four distinct skull morphotypes that are associated with specific burrowing techniques (Gans, 1974). We note that the use of "-snouted" versus "-headed" for these morphotypes varies in literature (e.g., Gans & Montero, 2008 for "-snouted" and Kearney, 2003 for "-headed"), but they convey the same concept. The "round-snouted" amphisbaenians (e.g., *Amphisbaena alba*) push their way through the substrate, compacting it to the sides of the tunnel with random head movements as they go. Amphisbaenians with other morphotypes employ more complicated methods. The "shovel-snouted" amphisbaenians (e.g., *Rhineura floridana*) burrow in two steps: first they ram their snout into the substrate, then they use the angled, horizontally-flattened top of their snout to compact the substrate to the top of the burrow. The "keel-snouted" amphisbaenians (e.g., *Anops kingii*) burrow similarly, but instead they use a vertical midline keel on their snout to compact the substrate to the right and left sides of the burrow. The "spade-snouted" amphisbaenians (e.g., *Agamodon anguliceps*) have skulls that superficially resemble those of the "shovel-snouted" amphisbaenians, but with an even flatter horizontal plane and strong margins. They burrow by rotating their heads around their longitudinal axis (i.e., roll), using the margins of the plane to shave substrate off the sides of the burrow. Intermediate forms exist between those morphotypes, representing extensive variation (Gans & Montero, 2008). With the exception of the "spade-snouted" amphisbaenians, which all belong to the monophyletic Trogonophidae, molecular evidence indicates that the other skull morphotypes do not correspond to monophyletic groups, and instead have repeatedly evolved in different clades (Gauthier et al., 2012; Kearney & Stuart, 2004; Pyron et al., 2013).

The various skull morphotypes suggest the potential for strong selective pressures acting on amphisbaenian skull morphology due to their HFB behavior. However, what is not well understood is how those selective pressures—and other factors that may interact with selective pressures such as ontogeny and sexual dimorphism—affect patterns of expressed morphology within a single species. Intraspecific variation in amphisbaenian skulls has not been examined closely, especially due to the rarity of amphisbaenian specimens. Most osteological descriptions for the clade are based on a single or few specimens (e.g., 1–12 specimens for the descriptions by Gans & Montero, 2008). Ontogenetic variation in the skull morphology of the "round-snouted" *Cynisca leucura* was described by Hipsley et al. (2016), and ontogenetic variation undoubtedly occurs in other amphisbaenians. Therefore, investigating intraspecific variation in the cranial osteology of other amphisbaenians will not only strengthen our understanding of amphisbaenian osteology, but could also reveal morphological constraints in other HFB vertebrate taxa because they face similar selective pressures due to their shared fossorial, HFB ecology.

We report intraspecific variation in the cranial osteology of the "spade-snouted" *Diplometopon zarudnyi* to expand knowledge of intraspecific variation in amphisbaenians. *Diplometopon* is a monotypic genus within Trogonophidae that inhabits western Iran, southern Iraq, Saudi Arabia, the United Arab Emirates, and western Oman (Behbehani et al., 2012). It can be found in open areas with loose soil or sand, even those that are disturbed by human activity (Behbehani et al., 2012). One population of adults was found to vary from 135 to 221 mm in snout-vent length and 148 to 236 mm in total length (Rudayni et al., 2017) and were dietary specialists on *Dermestes* larvae (Al-Sadoon et al., 2016). *Diplometopon zarudnyi* and other members of Trogonophidae exhibit acrodont dentition, while all other extant amphisbaenians exhibit pleurodont dentition (Kearney, 2003). The cranial osteology of *Diplometopon zarudnyi* was examined previously with both traditional methods (Abo-Eleneen et al., 2019; El-Assy & Al-Nassar, 1976; Gans, 1960) and with microcomputed tomography (microCT) (Maisano et al., 2006); however, those authors either addressed the osteology of a single specimen or did not investigate intraspecific variation closely. We utilized data from microCT scans of seven specimens of *Diplometopon zarudnyi* to explore and document variation in their cranial osteology. We hope that our findings can be used as a basis for future work on intraspecific variation in amphisbaenians, as well as other HFB vertebrate taxa.

2 | MATERIALS AND METHODS

Seven specimens of *Diplometopon zarudnyi* Nikolsky, 1907 from the Vertebrate Paleontology collection (TMM; formerly Texas Memorial Museum) at the University of Texas at Austin were X-ray microCT-scanned by Dr. Jessica Maisano at the University of Texas High-Resolution X-ray Computed Tomography Facility (UTCT) in a Xradia microXCT 400 scanner (ZEISS). The specimens were donated by the late Carl Gans and have no associated data, so results cannot be correlated with biogeography, habitat, and sex. However, it is likely that the specimens are from a single population or sampling event.

The specimens were originally formalin-fixed and fluid-preserved but are now desiccated, making traditional methods of skeletal preparation such as dissection, maceration, and cleaning with dermestid beetles difficult or impossible. All microCT data are available on MorphoSource under the project "*Diplometopon zarudnyi*" (https://www.morphosource.org/projects/000369111). See Table 1 for the scanning parameters and MorphoSource media identifiers for each specimen.

MicroCT has many advantages over traditional methods of examining cranial osteology. It is nondestructive and can reveal small, obscured, and internal structures. Those advantages are especially useful for amphisbaenians, because specimens are rare in collections and their skulls are often under 1 cm in length. Additionally, models generated from microCT data can be used to quantify morphological variation, therefore: (1) revealing variation that could not be detected by visual inspection alone and (2) allowing the correlation of morphological variation with other characteristics like biogeography, habitat, sex, and age to seek meaning in expressed intraspecific variation.

MicroCT data for each specimen were loaded into Mimics (version 20, Materialise) and segmented into individual skull elements by thresholding with the lasso tool and interpolation. The segmented elements were exported as three-dimensional (3D) models (.PLY). Whole skulls were reconstructed by loading all of the skull elements into MeshLab (version 2016.12, ISTI) and saving them as one model. No mirroring was used to create the skull models to preserve individual variation that may manifest as asymmetry.

The skull and disarticulated skull element models were first qualitatively examined by eye for intraspecific variation, such as extent of coossification and number of foramina. Extent of coossification was determined during microCT segmentation, as elements were segmented separately and therefore exported as separate models if they had complete internal sutures. We used 3D geometric morphometrics to quantify other forms of intraspecific variation. For the disarticulated skull elements, only the premaxilla, maxilla, frontal, and parietal were examined with 3D geometric morphometrics. Those elements were selected for quantitative examination because qualitative examination revealed that they had the most readily recognizable patterns of expressed variation (see Section 3).

In the first step of quantification, 3D landmarks were placed by hand on the skull models using Landmark Editor (version 3.0.0.6, Institute of Data Analysis and Visualization, UC Davis, USA). Nineteen landmarks were placed on prominent, homologous points across the entire skull (Figure 1). Variation among these landmarks was analyzed using the R-package *geomorph* v.3.2.1 (Adams & Otárola-Castillo, 2013). After loading the landmark data into *geomorph*, the landmarks were aligned with a generalized Procrustes analysis (Gower, 1975) using the function *gpagen*. Using the function *plotTangentSpace*, a principal component analysis (PCA) was run on the landmarks to quantify areas of variation by identifying principal components (PCs) and producing PCA plots.

TABLE 1 Scan parameters and MorphoSource media identifiers for specimens of *Diplometopon zarudnyi*

Specimen number	Date scanned	Voltage (kV)	Wattage (W)	Voxel size (μm)	Number of slices	Slice dimensions (px)	Slice file type	MorphoSource media identifiers
TMM M-11732	2014-01-08	90	10	6.23	1729	988 × 1010	.TIFF	000369114
TMM M-11733	2014-01-08	90	10	6.23	1765	988 × 1010	.TIFF	000370530
TMM M-11734	2014-01-08	90	10	6.23	1705	988 × 1010	.TIFF	000370539
TMM M-11735	2014-01-07	90	10	6.23	1730	988 × 1010	.TIFF	000370548
TMM M-11737	2012-09-26	70	10	9.57	1208	1012 × 1024	.TIFF	000370552
TMM M-11738	2012-09-26	70	10	9.57	1208	1012 × 1024	.TIFF	000370556
TMM M-11739	2012-09-26	70	10	10.80	1228	1012 × 1024	.TIFF	000370561

For the disarticulated skull element models, the R-package *auto3dgm* was used to automatically place 1000 pseudolandmarks across each element (Boyer et al., 2015). This automated method of landmarking was done rather than placing landmarks by hand because there were not enough prominent, homologous points on most skull elements to manually place landmarks and properly sample element shape. For paired elements (i.e., maxilla and frontal), pseudolandmarks were placed only on the element from the left side because left-right variation was already accounted for in visual inspection. Additionally, the premaxilla from TMM M-11737 and the maxillae from TMM M-11733 and TMM M-11737 were not included in the analyses because those elements were missing teeth and would have affected the PCA results. As *Diplometopon zarudnyi* has acrodont dentition, the teeth could not be reliably separated from their teeth-bearing elements and had to be included in the shape analyses of the premaxillae and maxillae. Landmark data from *auto3dgm* were analyzed using *geomorph* in the same way as the landmark data from Landmark Editor.

Measurements of the specimens, including total length, snout-vent length, maximum skull length, and maximum skull width, were taken using both physical and digital methods. Total length and snout-vent length were measured physically by running a tape measure along the skull and spine of the specimens because they are desiccated in nonlinear positions. Maximum skull length and skull width were digitally measured using the measurement tool in Mimics. Maximum skull length was taken as the greatest length, which was measured along the dorsal plane from the anteriormost point of the skull (anteroventral tip of premaxilla) to the posteriormost point of the skull (posterodorsal tip of otic-occipital complex or posteriormost point of occipital condyle, depending on the individual). Maximum skull width was also taken as the greatest width, which was measured along the transverse plane from the widest portion of the otic-occipital complex. These measurements are summarized in Table 2.

Selected areas of variation from both qualitative and quantitative analyses were tested for correlation with ontogenetic stage using the specimen measurements. Size can be used to infer ontogeny, although this method is unreliable with low sample numbers and produces results that are preliminary at best (Griffin et al., 2020). Additionally, without a way to infer ontogenetic stage, other factors such as sexual dimorphism could also be related to size (i.e., Rudayni et al., 2017). Nevertheless, a linear regression was performed using Minitab (version 19.2020.1, Minitab, LLC) for selected areas of variation versus snout-vent length and maximum skull length to test for allometry, and thus a possible ontogenetic influence on variation.

From the qualitative analysis, the selected areas of variation were: (1) number of foramina on the left frontal, (2) number of foramina on the left maxilla, and (3) extent of coossification of the occipital region. To score the extent of coossification of the occipital region, individuals were assigned 0 if they had no coossification of the occipital region, 1 if they had coossification between the

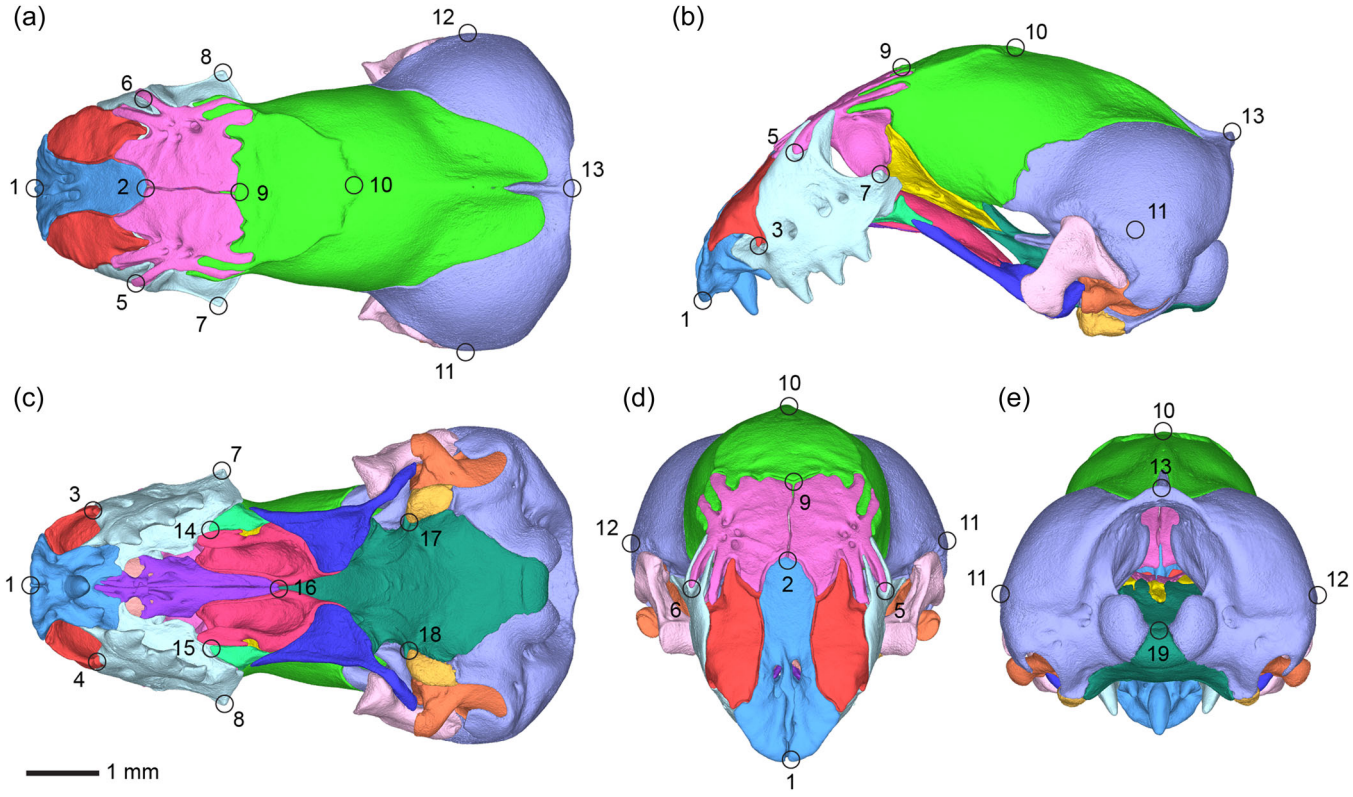

FIGURE 1 *Diplometopon zarudnyi* (TMM M-11732), placement of 19 landmarks on the skull for three-dimensional landmark-based geometric morphometrics in (a) dorsal view, (b) left lateral view, (c) ventral view, (d) anterior view, (e) posterior view. Anterior to the left in (a)–(c), ventral to the bottom in (d) and (e). Scale bar = 1 mm

TABLE 2 Intraspecific variation character states and general measurements for specimens of *Diplometopon zarudnyi*

Specimen number	Total length (mm)	Snout-vent length (mm)	Maximum skull length (mm)	Maximum skull width (mm)	Extent of coossification of the occipital region[a]	Frontal communicating foramina		Maxillary labial foramina		Premaxillary cleft
						Left	Right	Left	Right	
TMM M-11732	172	160	7.41	4.33	0	3	4	3	3	Present
TMM M-11733	188	180	7.71	4.74	1	2	3	3	2	Present
TMM M-11734	168	153	7.27	4.61	0	3	3	2	3	Absent
TMM M-11735	178	160	7.71	4.52	0	4	2	3	2	Absent
TMM M-11737	215	195	8.18	4.91	2	3	4	3	3	Absent
TMM M-11738	170	158	7.63	4.61	0	2	3	3	2	Absent
TMM M-11739	215	198	8.76	5.46	1	3	3	3	3	Present

[a]0 = no coossification, 1 = coossification between the parabasisphenoid-basioccipital complex and otic-occipital complex, and 2 = coossification between the parabasisphenoid-basioccipital complex, otic-occipital complex, and elements X.

"parabasisphenoid-basioccipital complex" (see Section 3) and otic-occipital complex, and 2 if they had coossification between the parabasisphenoid-basioccipital complex, otic-occipital complex, and elements X (cranial sesamoid, see Montero et al., 2017 for discussion). From the quantitative analysis, PC scores from the skull and examined skull elements were used in the linear regression.

3 | RESULTS

3.1 | Qualitative analysis

Four areas of intraspecific variation were discernible without the use of quantitative shape analysis. These include: (1) the shape of the rostral blade of the premaxilla; (2) the number, shape, and position of foramina of the premaxilla, frontals, and maxillae; (3) the pattern of interdigitation between the frontals and parietal; and (4) the extent of coossification of the occipital region. Table 2 summarizes the states for those areas of variation in addition to general skull measurements for each specimen. Terminology for foramina and processes follows Maisano et al. (2006; Figure 2).

The rostral blade of the premaxilla varies in shape due to the presence or absence of a medial cleft. When present, this cleft extends from the edge of the rostral blade to the anterior end of the ridge between the dorsal rostral foramina, sometimes even extending ventral to the ridge for a short distance. This cleft is present in three specimens (TMM M-11732, TMM M-11733, and TMM M-11739) and absent in the remaining four specimens studied (Figure 3a).

The paired dorsal rostral foramina and the surrounding region on the anterodorsal surface of the premaxilla are variable in two ways (Figure 3a). First, the foramina themselves vary in the extent of the opening and are sometimes subdivided (e.g., TMM M-11734), often creating left-right asymmetry. Second, the raised ridge of bone between the two dorsal rostral foramina varies in shape. In most specimens it smoothly connects anteriorly to the rostral blade and posteriorly to the nasal process of the premaxilla, but in TMM M-11734 that connection is interrupted and makes the ridge longer dorsally than ventrally. In TMM M-11735 the ridge has dorsal gaps, and in TMM M-11733 there is a lateral hole. In TMM M-11735 and TMM M-11739 the ridge bridges laterally across the dorsal rostral foramen to connect to the rest of the premaxilla. There is also a bridge in TMM M-11734, but it occurs at the same level as the rest of the premaxilla rather than originating from the top of the ridge. This bridging was only present on one side in all three cases, again causing left-right asymmetry.

Foramina on the maxillae and frontals vary in number, size, and position. For the maxillae, there are two to three labial foramina on each element (Figure 3b). When a third labial foramen is present it is often much smaller than the other two and is positioned between them. For the frontals, there are two to four communicating foramina on each element (Figure 3c). For both elements, the number of foramina on the left and right frontal or maxilla can differ, introducing left-right asymmetry (Table 2).

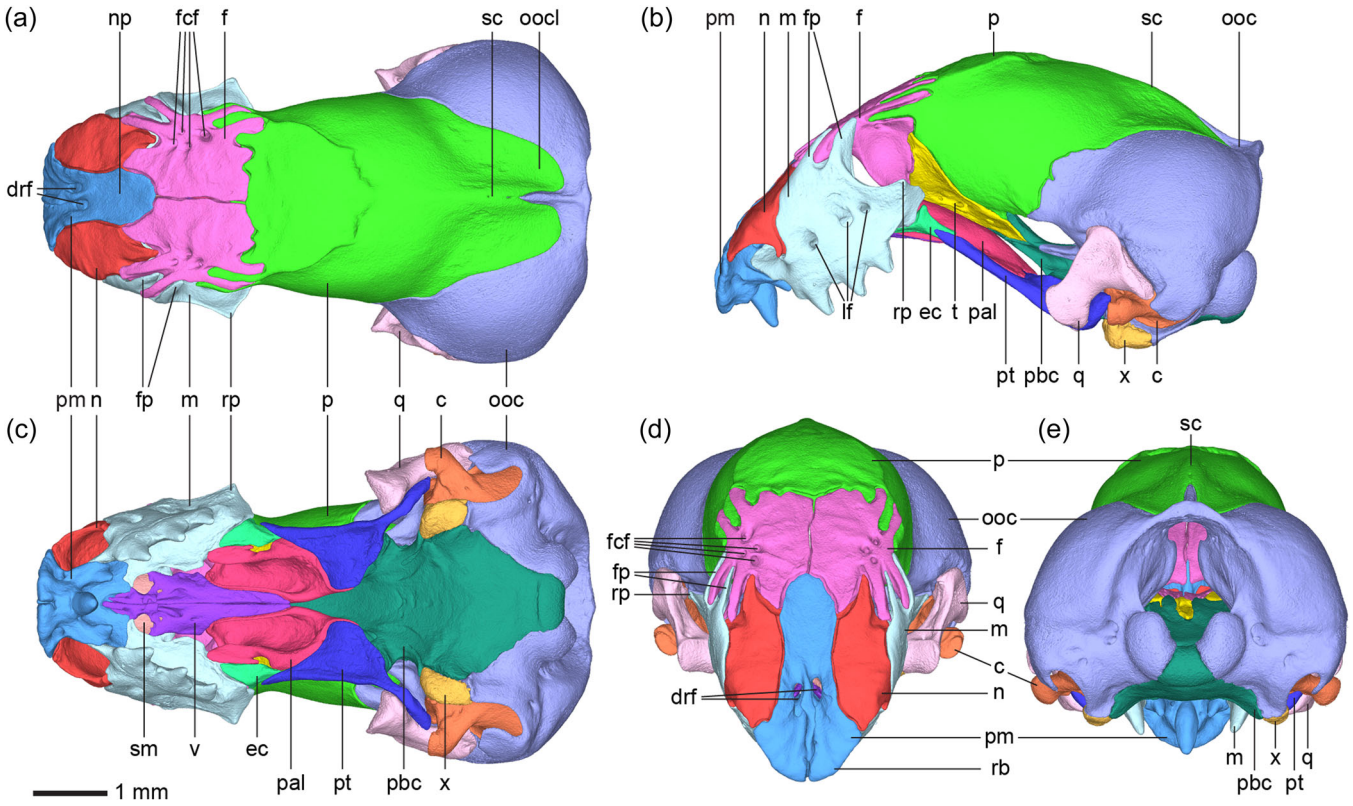

FIGURE 2 *Diplometopon zarudnyi* (TMM M-11732), three-dimensional recreation of the skull in (a) dorsal view, (b) left lateral view, (c) ventral view, (d) anterior view, (e) posterior view. Anterior to the left in (a)–(c), ventral to the bottom in (d) and (e). Scale bar = 1 mm. c, columella; drf, dorsal rostral foramina; ec, ectopterygoid; f, frontal; fcf, frontal communicating foramina; fp, frontal processes; lf, labial foramina; m, maxilla; n, nasal; np, nasal process; ooc, otic-occipital complex; oocl, otic-ocipital lappet; p, parietal; pal, palatine; pbc, parabasisphenoid-basioccipital complex; pm, premaxilla; pt, pterygoid; q, quadrate; rb, rostral blade; rp, rostral process; sc, sagittal crest (present but barely visible in this individual); sm, septomaxilla; t, tabulosphenoid (=orbitosphenoid of Maisano et al., 2006); v, vomer; x, element X

The pattern of the frontal-parietal interdigitation varies among individuals and is more often than not left-right asymmetrical (Figure 4). The interdigitation is shallow medially, becoming longer as the suture progresses laterally and results in interlocking, finger-like processes on both the frontals and the parietal. The medial portion is not as shallow in some individuals and may have small processes, but these processes are not as large and long as those in the lateral portion. Consistently counting the number of processes in the interdigitation for each specimen is not feasible due to the extent of variation; however, there is an observable difference in the number, not only among individuals but also between the left and right sides of the same individual. Notably, although the frontal-parietal interdigitation is variable, the frontal-maxilla-nasal interdigitation is far more conserved. The shape and number of processes in the latter location is constant across all individuals.

The extent of coossification of the otic-occipital complex varies among individuals (Figure 5). In most cases the parabasisphenoid and basioccipital are fused into one element (here termed the "parabasisphenoid-basioccipital complex") and remain separate from the otic-occipital complex and the elements X. However, in some specimens more fusion is present. In two specimens (TMM M-11733 and TMM M-11739) the parabasisphenoid-basioccipital complex is fused with the rest of the otic-occipital complex but the elements X remain free. In one individual (TMM M-11737) there is complete fusion between the parabasisphenoid-basioccipital complex, otic-occipital complex, and elements X. The specimens with partial or complete fusion of the occipital region are also the largest specimens in the sample.

3.2 | Quantitative analysis

Using 3D geometric morphometrics, the skull and select individual skull elements (premaxilla, maxilla, frontal, and parietal) were examined for intraspecific variation not easily discerned by visual inspection. All PCA output is summarized in Table 3.

3.2.1 | Skull

For the skull, the PCA revealed shape variation in the angle of the rostrum and the distance between the elements X (Figure 6). PC 1 (37.8% of variation) showed that the ventral angle of the rostrum is smaller (i.e., more ventrally-projected) on the negative end of

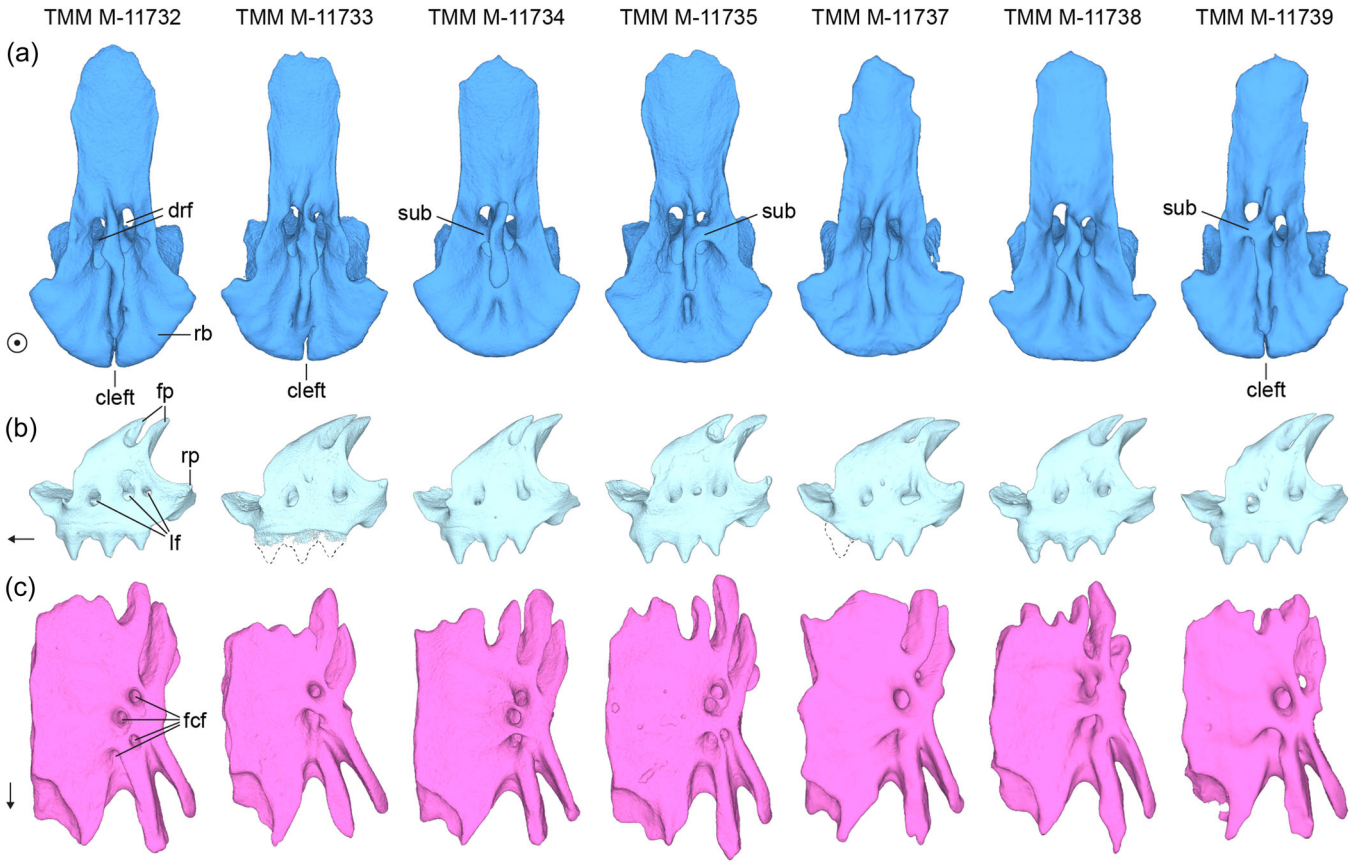

FIGURE 3 *Diplometopon zarudnyi*, (a) Premaxillae, anterior view with ventral to the bottom. (b) Left maxillae, left lateral view with anterior to the left. (c) Left frontals, dorsal view with anterior to the bottom. Intraspecific variation is visible in the shape of the dorsal rostral foramina and the presence or absence of a rostral blade cleft in the premaxillae. Similarly, the number, size, and placement of the labial foramina in the maxillae and frontal communicating foramina in the frontals varies. drf, dorsal rostral foramina; fcf, frontal communicating foramina; fp, frontal processes; lf, labial foramina; rb, rostral blade; rp, rostral process; sub, subdivided dorsal rostral foramen

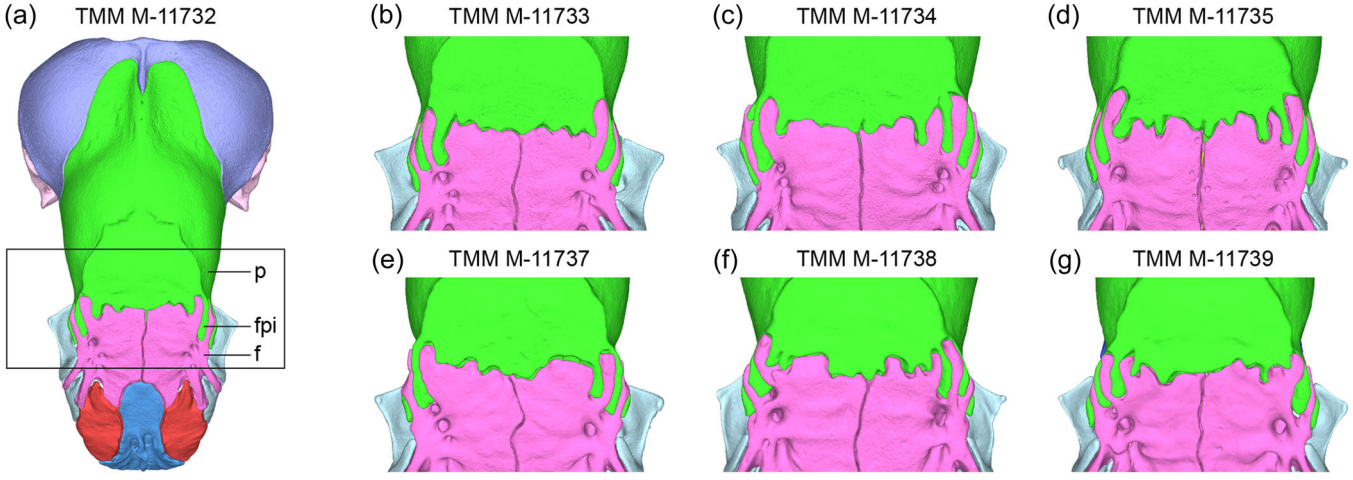

FIGURE 4 *Diplometopon zarudnyi*, intraspecific variation in frontal-parietal interdigitation among specimens. (a) TMM M-11732, dorsal view with anterior to the bottom. Area of interdigitation between the frontals and parietal is boxed in (a): f, frontal; fpi, frontal-parietal interdigitation; p, parietal. (b–g) Frontal-parietal interdigitation in other specimens. Dorsal view with anterior to the bottom. Intraspecific variation is visible in the pattern of frontal-parietal interdigitation, specifically left-right symmetry as well as number, shape, and length of the processes as figured in pink and green

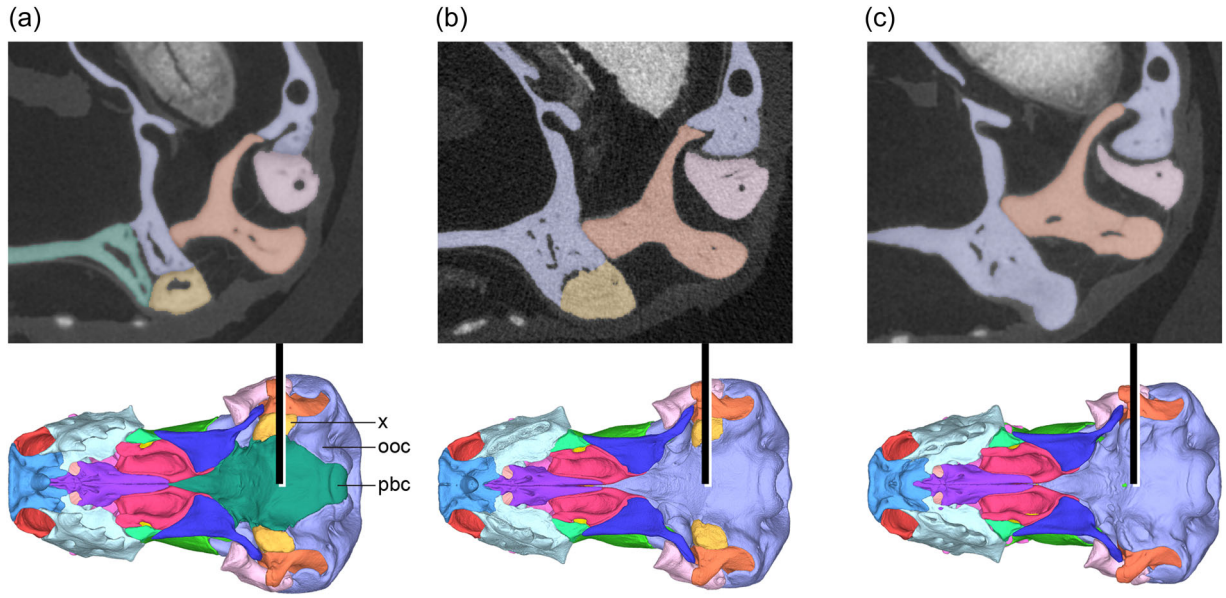

FIGURE 5 *Diplometopon zarudnyi*, transverse CT slices from the left ventral portion of the occipital region show varying extent of coossification in the occipital region. (a) TMM M-11738 shows no coossification between the oto-occipital complex, parabasisphenoid-basioccipital complex, and elements X. (b) TMM M-11733 shows coossification between the oto-occipital complex and parabasisphenoid-basioccipital complex. (c) TMM M-11737 shows coossification between the oto-occipital complex, parabasisphenoid-basioccipital complex, and elements X. ooc, otic-occipital complex; pbc, parabasisphenoid-basioccipital complex; x, element X

TABLE 3 Principal component analysis (PCA) results from three-dimensional (3D) geometric morphometrics of skull and individual skull elements

Element	Statistic	PC 1	PC 2	PC 3	PC 4	PC 5	PC 6
Skull	Standard deviation	0.02026	0.01584	0.01333	0.01041	0.009501	0.007017
	Proportion of variance	0.37759	0.23087	0.16353	0.09967	0.083050	0.045290
	Cumulative proportion	0.37759	0.60846	0.77199	0.87166	0.954710	1.000000
Premaxilla	Standard deviation	0.06037	0.03764	0.02926	0.02429	0.02296	
	Proportion of variance	0.51810	0.20140	0.12168	0.08389	0.07492	
	Cumulative proportion	0.51810	0.71950	0.84119	0.92508	1.00000	
Maxilla	Standard deviation	0.06033	0.0395	0.03668	0.02498		
	Proportion of variance	0.50770	0.2177	0.18762	0.08703		
	Cumulative proportion	0.50770	0.7254	0.91297	1.00000		
Frontal	Standard deviation	0.05902	0.04625	0.03342	0.02919	0.02449	0.01955
	Proportion of variance	0.40632	0.24945	0.13028	0.09941	0.06997	0.04456
	Cumulative proportion	0.40632	0.65577	0.78606	0.88547	0.95544	1.00000
Parietal	Standard deviation	0.05468	0.03333	0.02663	0.02316	0.02085	0.01976
	Proportion of variance	0.48451	0.17999	0.11491	0.08689	0.07041	0.06329
	Cumulative proportion	0.48451	0.66450	0.77941	0.86630	0.93671	1.00000

the PC 1 axis, and larger (i.e., less ventrally-projected) on the positive end. On the negative end of PC 2 (23.1% of variation) were skulls with elements X relatively far apart, and on the positive end were skulls with elements X relatively close together.

3.2.2 | Skull elements

For the premaxilla, the PCA revealed shape variation in the nasal process (Figure 7). On the negative end of the PC 1 axis (51.8% of variation) were premaxillae with laterally-constricted nasal processes

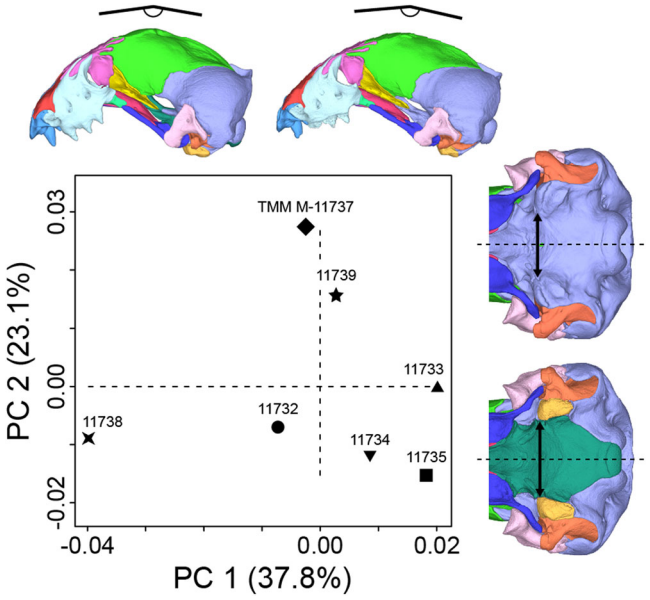

FIGURE 6 Principal component analysis plot for the skulls of *Diplometopon zarudnyi*. PC 1 (37.8% of variation) shows a small ventral angle of the rostrum on the negative end, and a large ventral angle of the rostrum on the positive end. Pictured for PC 1 are the skulls of TMM M-11738 to the left and TMM M-11733 to the right in left lateral view, anterior to the left. PC 2 (23.1% of variation) shows elements X relatively far apart on the negative end, and elements X relatively close together on the positive end. Pictured for PC 2 are the occipital regions of TMM M-11737 above and TMM M-11735 below in ventral view, anterior to the left

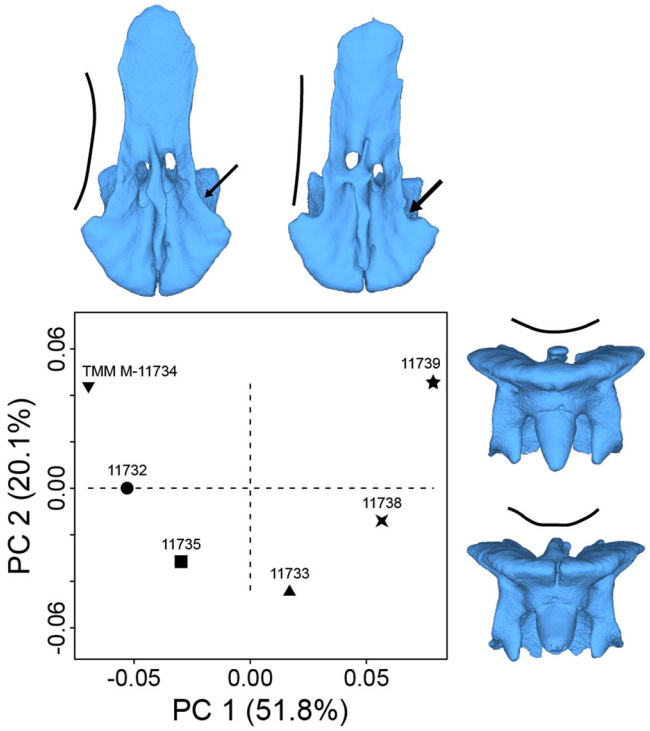

FIGURE 7 Principal component analysis plot for the premaxillae of *Diplometopon zarudnyi*. PC 1 (51.8% of variation) shows a laterally constricted nasal process and weak notches at the border between the nasal process and rostral blade on the negative end, and an unconstricted nasal process and strong notches on the positive end. Pictured for PC 1 are the premaxillae of TMM M-11732 to the left and TMM M-11739 to the right in anterior view, ventral to the bottom. PC 2 (20.1% of variation) shows a relatively more concave dorsal surface on the negative end, and a relatively less concave dorsal surface on the positive end. Pictured for PC 2 are the premaxillae of TMM M-11734 above and TMM M-11733 below in ventral view, anterior to the top

and weak notches at the border between the nasal process and rostral blade, and on the positive end were premaxillae with unconstricted nasal processes and strong notches. Curiously, the premaxilla of TMM M-11734 was the most negatively-placed premaxilla despite lacking lateral constriction on the nasal process. On the negative end of the PC 2 axis (20.1% of variation) were premaxillae with relatively more concave dorsal surfaces, and on the positive end were premaxillae with relatively less concave dorsal surfaces.

For the maxilla, the PCA revealed shape variation in the frontal processes and rostral process (Figure 8). On the negative end of the PC 1 axis (50.8% of variation) were maxillae with relatively short and less posteriorly-projected frontal processes, and on the positive end were maxillae with relatively long and more posteriorly-projected frontal processes. On the negative end of the PC 2 axis (21.8% of variation) were maxillae with a relatively weak rostral process, and on the positive end were maxillae with a relatively strong rostral process. Lastly, on the negative end of the PC 3 axis (18.8% of variation) were maxillae with frontal processes that are relatively far apart, and on the positive end were maxillae with frontal processes that are relatively close together.

For the frontal, the PCA revealed shape variation in the posterior processes involved in the frontal-parietal interdigitation (Figure 9). On the negative end of the PC 1 axis (40.6% of variation) were frontals with two major processes, and on the positive end were frontals with three major processes. On the negative end of the PC 2 axis (25.0% of variation) were frontals with relatively short posterior processes, and on the positive end were frontals with relatively long posterior processes.

For the parietal, the PCA revealed shape variation in the sagittal crest and otic-occipital lappet (Figure 10). On the negative end of the PC 1 axis (48.5% of variation) were parietals with a relatively weak sagittal crest and more ventrally-projected otic-occipital lappet, and on the positive end were parietals with a relatively strong sagittal crest and less ventrally-projected otic-occipital lappet. On the negative end of the PC 2 axis (18.0% of variation) were parietals with a relatively narrow otic-occipital lappet, and on the positive end were parietals with a relatively wide otic-occipital lappet. Lastly, on the negative end of the PC 3 axis (11.5% of variation) were parietals with a relatively long posterior notch in their otic-occipital lappet, and on the positive end were parietals with a relatively short posterior notch in their otic-occipital lappet.

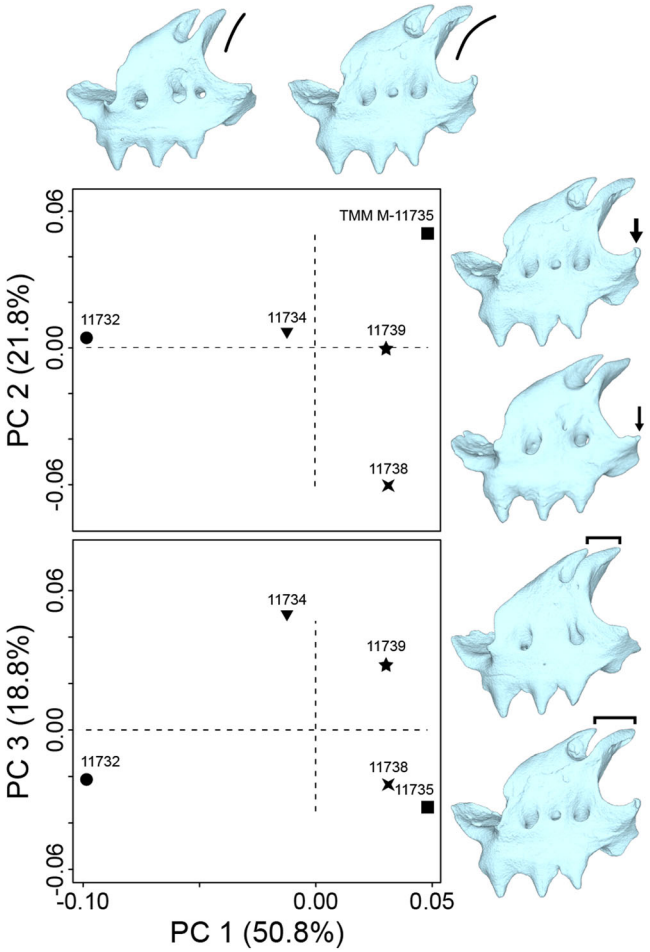

FIGURE 8 Principal component analysis plots for the left maxillae of *Diplometopon zarudnyi*. PC 1 (50.8% of variation) shows relatively short and less posteriorly-projected frontal processes on the negative end, and relatively long and more posteriorly-projected frontal processes on the positive end. Pictured for PC 1 are the left maxillae of TMM M-11732 to the left and TMM M-11735 to the right in left lateral view, anterior to the left. PC 2 (21.8% of variation) shows a relatively weak rostral process on the negative end, and a relatively strong rostral process on the positive end. Pictured for PC 2 are the left maxillae of TMM M-11735 above and TMM M-11738 below in left lateral view, anterior to the left. PC 3 (18.8% of variation) shows frontal processes that are relatively far apart on the negative end, and frontal processes that are relatively close together on the positive end. Pictured for PC 3 are the left maxillae of TMM M-11734 above and TMM M-11735 below in left lateral view, anterior to the left

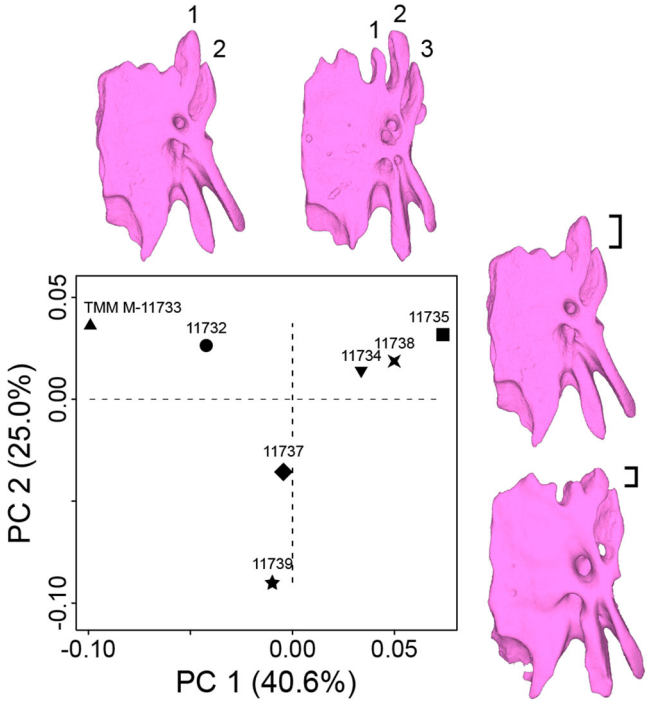

FIGURE 9 Principal component analysis plot for the left frontals of *Diplometopon zarudnyi*. PC 1 (40.6% of variation) shows two major posterior processes on the negative end, and three major posterior processes on the positive end. Pictured for PC 1 are the left frontals of TMM M-11733 to the left and TMM M-11735 to the right in dorsal view, anterior to the bottom. PC 2 (25.0% of variation) shows relatively short posterior processes on the negative end, and relatively long posterior processes on the positive end. Pictured for PC 2 are the left frontals of TMM M-11733 above and TMM M-11739 below in dorsal view, anterior to the bottom

3.3 | Correlation of selected areas of variation with size

The specimens of *Diplometopon zarudnyi* ranged from 153 to 198 mm for snout-vent length and 168 to 215 mm for total length, which is consistent with the adult length measurements by Rudayni et al. (2017) despite the desiccated state of the specimens in our sample. To control for the potential effect of desiccation on snout-vent length and total length, maximum skull length and width were also measured and ranged from 7.27 to 8.76 mm and 4.33 to 5.46 mm, respectively.

A linear regression with both snout-vent length and maximum skull length was performed on the number of foramina on the left frontal, number of foramina on the left maxilla, extent of coossification of the occipital region, and PC scores from the skull and examined skull elements. Of those regressions, the following had significant results: extent of coossification of the occipital region, skull PC 2, frontal PC 2, and parietal PC 1.

Snout-vent length was positively correlated with increasing coossification of the occipital region ($p = .005$; Figure 11a). Maximum skull length also was positively correlated with increasing coossification of the occipital region, but that correlation was not significant ($p = .105$; Figure 11b). Both snout-vent length ($p = .002$; Figure 11c) and maximum skull length ($p = .040$; Figure 11d) were positively correlated with skull PC 2, meaning that as size increases the distance between the elements X decreases. Similarly, both snout-vent length ($p = .041$; Figure 11e) and maximum skull length ($p = .007$; Figure 11f) were negatively correlated with frontal PC 2, meaning that as size increases the length of the posterior processes decreases. Lastly, snout-vent length was positively correlated with parietal PC 1

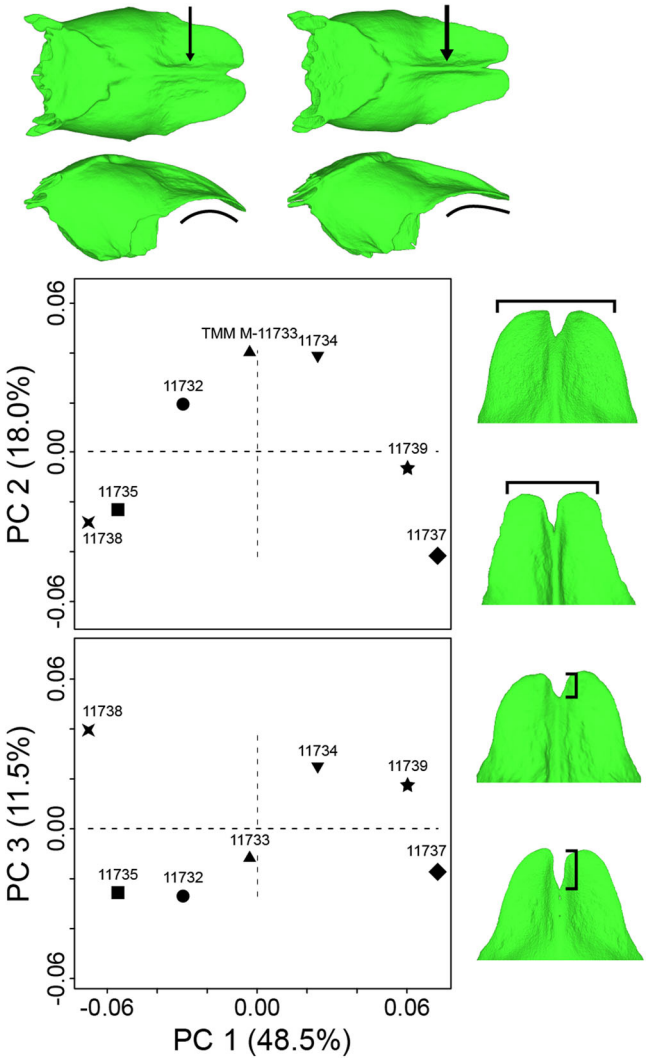

FIGURE 10 Principal component analysis plots for the parietals of *Diplometopon zarudnyi*. PC 1 (48.5% of variation) shows a relatively weak sagittal crest and more ventrally-projected otic-occipital lappet on the negative end, and a relatively strong sagittal crest and less ventrally-projected otic-occipital lappet on the positive end. Pictured for PC 1 are the parietals of TMM M-11738 to the left and TMM M-11737 to the right in dorsal view above and left lateral view below, anterior to the left. PC 2 (18.0% of variation) shows a relatively narrow otic-occipital lappet on the negative end, and a relatively wide otic-occipital lappet on the positive end. Pictured for PC 2 are the otic-occipital lappets of TMM M-11733 above and TMM M-17737 below in dorsal view, anterior to the bottom. PC 3 (11.5% of variation) shows a relatively long posterior notch in the otic-occipital lappet on the negative end, and a relatively short posterior notch on the positive end. Pictured for PC 3 are the otic-occipital lappets of TMM M-11738 above and TMM M-11732 below in dorsal view, anterior to the bottom

(p = .046; Figure 11g), meaning that as size increases the sagittal crest is stronger and otic-occipital lappet is less ventrally-projected. Maximum skull length also was positively correlated with parietal PC 1, but that correlation was not significant (p = .151; Figure 11h).

4 | DISCUSSION

The HFB behavior of amphisbaenians likely places strong selective pressures on their cranial morphology, as evidenced by the wide range of skull morphotypes in amphisbaenians that are paired with different methods of HFB (Gans, 1974). The existence of multiple, though similar, head morphologies scattered across the phylogeny of the group demonstrates that multiple evolutionary "solutions" to various pressures were achieved. Selection is not shaping amphisbaenian skulls towards some singular "ideal" or "optimal" morphotype. Although selective pressures due to HFB behavior were hypothesized to affect skull morphology across amphisbaenian species, what has not been thoroughly examined is how selective pressures or other factors such as ontogeny and sexual dimorphism shape skull morphology within the same species. Through microCT data and 3D landmark-based geometric morphometrics, we were able to investigate the skulls and skull elements of *Diplometopon zarudnyi* for morphological intraspecific variation in more detail than ever before, providing a valuable reference for others studying amphisbaenians and HFB taxa.

Intraspecific variation was found in the shape of the rostral blade of the premaxilla, the number and placement of foramina, the pattern of frontal-parietal interdigitation, and the extent of coossification of the occipital region. 3D landmark-based geometric morphometrics also revealed differences in the angle of the rostrum and the shape of all individual skull elements we examined (premaxilla, maxilla, frontal, and parietal). Our morphometric results were difficult to interpret but this was to be expected because of the subtle nature of intraspecific variation, especially with a small sample size of seven specimens of unknown age and sex.

4.1 | Comparison to past studies

Previous authors who studied the skulls of *Diplometopon zarudnyi* reported morphological features that are consistent with the intraspecific variation we found in this study. Two labial foramina on the maxilla and a fully coossified otic-occipital complex in adult specimens were previously reported by Gans (1960). The basioccipital was reported to be a separate element from the rest of the otic-occipital complex by El-Assy and Al-Nassar (1976) and Abo-Eleneen et al. (2019). Both sets of authors also reported a suture between the parabasisphenoid and basioccipital, something we did not observe in our sample. A subdivided dorsal rostral foramen on the premaxilla, premaxilla with no cleft, two communicating foramina on each frontal, two labial foramina on each maxilla, and a fully coossified occipital region were reported for the single specimen of *Diplometopon zarudnyi* studied by Maisano et al. (2006; Field Museum of Natural History FMNH 64429). Those observations demonstrate that there are even more variant conditions in *Diplometopon zarudnyi* than seen in our sample.

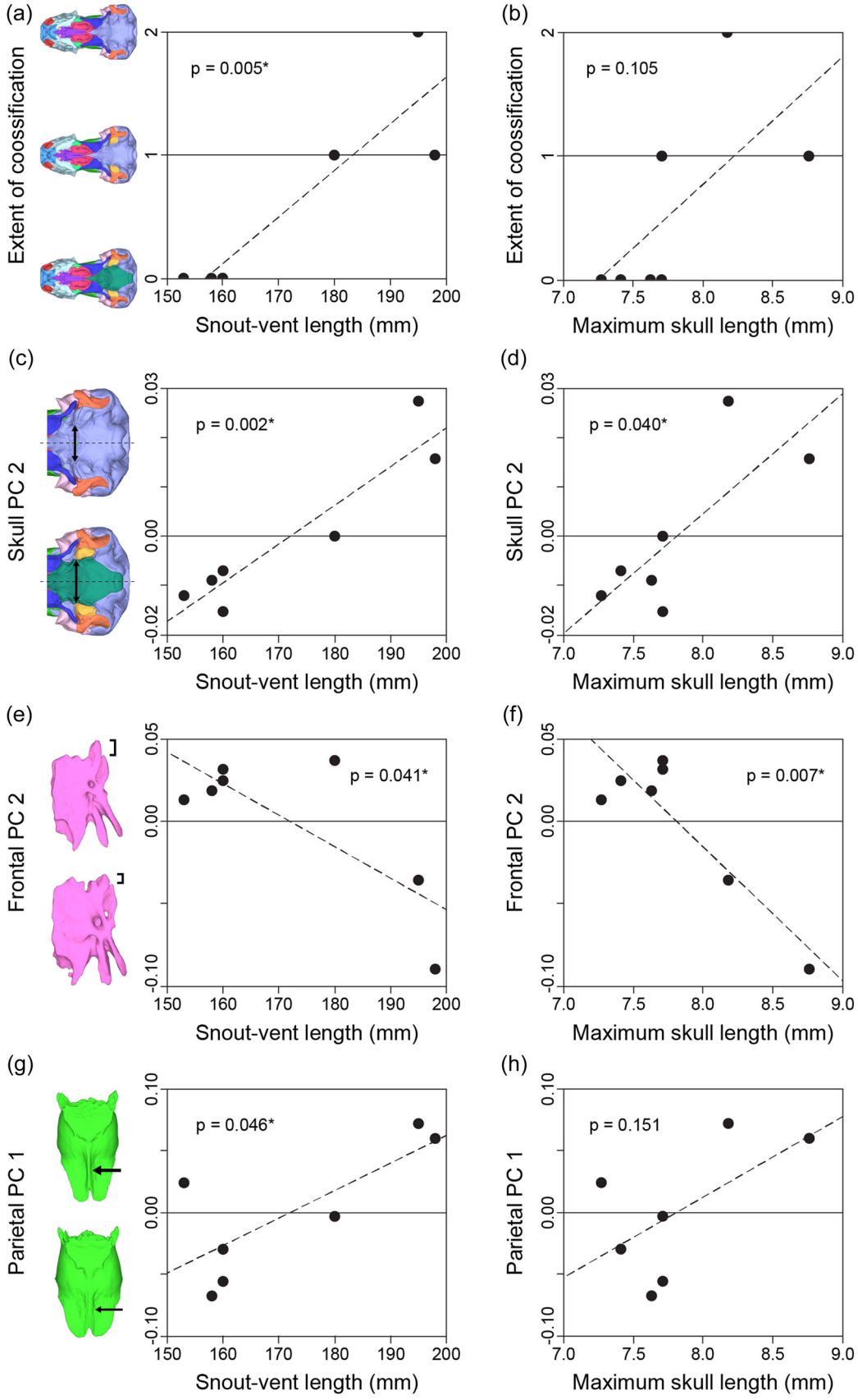

FIGURE 11 (See caption on next page)

4.2 | Potential influences on variation

The observed areas of intraspecific variation could be explained by a variety of causes, including but not limited to biomechanics and ontogeny. Due to their HFB behavior, biomechanics undoubtedly plays an important role in driving the evolution of the skull morphology in *Diplometopon zarudnyi*. Their skulls must be structured to handle the forces imposed on them from burrowing, especially torsional forces because this "spade-snouted" taxon burrows by rotating its head dorsally and ventrally (Gans, 1974). Even small changes in skull shape are likely to influence biomechanics because of the importance of the skull for burrowing.

Like biomechanics, ontogeny also influences skull morphology through associated skeletal changes. Ontogenetic variation in the skull of the amphisbaenian *Cynisca leucura* (Amphisbaenidae) was reported by Hipsley et al. (2016). They found that adults had a more slender, dorsoventrally-compressed postorbital region and a higher degree of interdigitation than juveniles. The ontogeny of amphisbaenian skulls has not been investigated much beyond this, but the results from Hipsley et al. (2016) show the potential for similar findings in other amphisbaenian taxa. We explore the influence of biomechanics and ontogeny below for the most notable areas of intraspecific variation.

4.2.1 | Interdigitation

One way that amphisbaenian skulls resist burrowing forces is through interdigitated cranial sutures, which have long interlocking processes that improve stability between bones (Gans, 1978). Interdigitation is present in *Diplometopon zarudnyi* in the frontal-maxilla-nasal sutures and frontal-parietal suture. Because interdigitation is important for burrowing in amphisbaenians, the intraspecific variation observed in the frontal-parietal suture may have biomechanical implications.

One hypothesis is that the interdigitated sutures in Trogonophidae seem to follow the tension lines imposed by torsion during burrowing (Gans, 1974). As such, variation in interdigitation is possibly driven by differences in these tension lines. The conserved nature of the frontal-maxilla-nasal interdigitation versus the variable nature of the frontal-parietal interdigitation presents two possibilities under the explanation of tension lines. The first possibility occurs if the frontal-maxilla-nasal interdigitation is placed under greater tension during burrowing than the frontal-parietal interdigitation. In this case, the frontal-maxilla-nasal interdigitation is conserved because any morphological change would diminish its ability to resist tension from burrowing, whereas the frontal-parietal interdigitation is variable because many different morphological states can resist the weaker tension it experiences. The second possibility occurs if the frontal-parietal interdigitation is placed under greater tension during burrowing than the frontal-maxilla-nasal interdigitation. In this case, the frontal-parietal interdigitation is variable due to being restructured to finely match the tension lines imposed on it, whereas the frontal-maxilla-nasal interdigitation is conserved because there is no restructuring under weaker tension. The alternative explanations could be investigated by simulating burrowing stress on skulls through finite element analysis.

The variation in frontal-parietal interdigitation could also be a response to muscle-induced loading. Muscle-bone interactions affect skull morphology and are important for proper skull development, such that different muscle-induced loadings result in different skull morphologies (Conith et al., 2019). Therefore, the muscles responsible for burrowing may "pull" on the frontal-parietal interdigitation, influencing the shape and number of processes. That muscle-bone interaction could also explain why the processes increase in length laterally, because one muscle likely to be involved in head rotation during burrowing, the *M. cervicomandibularis*, inserts on the anterior dorsolateral side of the parietal (Al-Hassawi, 2004). Al-Hassawi (2004) did not report muscles that insert on the frontal, maxilla, or nasal, so the lack of muscles "pulling" in that region may explain the conserved nature of the frontal-maxilla-nasal interdigitation in comparison to the variable nature of the frontal-parietal interdigitation.

However, the variation in frontal-parietal interdigitation may not be in response to anything and instead could be random variation after meeting a minimum condition in skull structure that is adequate to allow survival under the torsion and strain from burrowing (Gans, 1993). As noted by Gans (1993), adaptations are not guaranteed to perfectly match current environmental conditions due to phenotypic and environmental variation, as well as the cost of adaptations incurring tradeoffs. Therefore, because individuals would tend to survive with morphological features that are at least adequate for the conditions in which they live, true optimization of adaptions is rare (Gans, 1993). Applying this principle to *Diplometopon zarudnyi* means that the frontal-parietal interdigitation likely has a minimum condition where it is adequate for burrowing forces, beyond which the interdigitation varies randomly with no recognizable pattern.

Diplometopon zarudnyi is not the only amphisbaenian that varies in its interdigitation. *Amphisbaena alba* (Amphisbaenidae) shows similar differences between individuals and bilaterally within the same individual (Gans & Montero, 2008). Additionally, although not directly addressed in the literature, bilateral variation in interdigitation is visible in other amphisbaenian skulls, such as *Geocalamus*

FIGURE 11 Linear regressions of snout-vent length and maximum skull length versus selected areas of variation: (a, b) extent of coossification of the occipital region, where 0 = no coossification, 1 = coossification between the parabasisphenoid-basioccipital complex and otic-occipital complex, and 2 = coossification between the parabasisphenoid-basioccipital complex, otic-occipital complex, and elements X; (c, d) skull PC 2; (e, f) frontal PC 2; and (g, h) parietal PC 1

acutus (Gans & Montero, 2008: figure 3.34). Those examples show that the phenomenon may apply to other amphisbaenians and perhaps other HFB taxa with sutural interdigitation.

Variation in the frontal-parietal interdigitation may also be explained by ontogenetic changes in skull architecture. As mentioned above, ontogenetic variation in the degree of frontal-parietal interdigitation in *Cynisca leucura* was reported by Hipsley et al. (2016), with adults having longer, more medially-directed and anteriorly-placed interdigitation processes than juveniles. Unlike *Cynisca leucura*, the frontal-parietal interdigitation processes in *Diplometopon zarudnyi* may shorten with age, as evidenced by the negative, significant correlation between size and frontal PC 2 (representing the length of the posterior processes). The shortening rather than lengthening of processes with age may be because the "spade-snouted" *Diplometopon zarudnyi* practices a different method of HFB than the "round-snouted" *Cynisca leucura* and, as such, has different biomechanical pressures on its interdigitated sutures. However, the unreliability of inferring ontogeny from size at such low sample numbers hinders this finding. Additionally, the specimens in our study appear to be adults as indicated by their snout-vent length and total length measurements matching the adult measurements reported by Rudayni et al. (2017), so our sample is likely missing the earlier ontogenetic stages needed to confirm that interdigitation processes shorten with age.

4.2.2 | Occipital region coossification

The variable extent of coossification of the occipital region likely has ties to ontogeny. Coossification of bones occurs with age throughout vertebrate taxa, such as the fusion of epiphyses to diaphyses in long bones and the fusion of various cranial bones (e.g., Maisano, 2002). Fusion of the occipital region between the supraoccipital, exoccipitals, basioccipital, prootic, and supratemporals was previously reported in the trogonophid amphisbaenian *Trogonophis wiegmanni* (Gans & Montero, 2008). In juveniles, those bones tend to be independent, but in adults they tend to be fused together, showing evidence of ontogenetic variation (Gans & Montero, 2008). Although the variation in coossification seen in *Diplometopon zarudnyi* is between different bones—parabasisphenoid, basioccipital, elements X, and the otic-occipital complex—the precedence of similar fusion happening through ontogeny in related taxa suggests that ontogenetic change explains the variation in our sample. Additionally, size-dependent fusion of the elements X to surrounding bone was also observed in *Amphisbaena bolivica* (Amphisbaenidae) by Montero et al. (2017).

For our sample, ontogenetic variation in the occipital region is supported by the positive, significant correlation between snout-vent length and extent of coossification of the occipital region. Additionally, the positive, significant correlation between both snout-vent length and maximum skull length with skull PC 2—representing the distance between the elements X—may be related to the fusion of the elements X to the otic-occipital complex with age. However, these findings are hindered by the same caveats discussed above for interdigitation, in addition to the positive but not significant correlation between maximum skull length and extent of coossification of the occipital region.

If extent of coossification is indeed tied to ontogeny, then based on our results and those of El-Assy and Al-Nassar (1976) and Abo-Eleneen et al. (2019), the sequence of postnatal coossification of the otic-occipital complex appears to be: (1) the parabasisphenoid fuses to the basioccipital forming the parabasisphenoid-basioccipital complex, (2) the parabasisphenoid-basioccipital complex fuses to the otic-occipital complex, and (3) the elements X fuse to the otic-occipital complex. This aligns with observations by Maisano (2002), who reported a similar ontogenetic sequence of the basisphenoid fusing to the basioccipital and then the basioccipital fusing to the otooccipital in *Callisaurus draconoides* and *Uta stansburiana* (Iguania: Phrynosomatidae).

The extent of coossification of the occipital region also influences biomechanics by changing the number of sutures in the skull. Sutures without joints or interdigitation—like those seen in the occipital region—are relatively weak points in the mechanical structure of the skull (Preuschoft & Witzel, 2002). Bite force simulations on a skull of *Sphenodon* showed that the presence of sutures generates widely-distributed, high levels of strain throughout the skull (Curtis et al., 2013). Similarly, muscle-, bite-, and joint-force simulations on a skull of *Uromastyx hardwickii* revealed that individual sutures relieve strain locally at the cost of elevated strain elsewhere in the skull, with all sutures working together to distribute strain throughout the skull (Moazen et al., 2009). High levels of strain are not necessarily harmful and may be important for proper bone growth (Curtis et al., 2013; Moazen et al., 2009). Although the effect of sutures on bite-force distribution has been investigated, there is far less research on the effect of sutures on the distribution of forces resulting from burrowing, which may be more relevant to HFB taxa like *Diplometopon zarudnyi*.

4.2.3 | Rostrum angle

Variation in the angle of the rostrum has biomechanical implications as well. The angle reflects two structural requirements in the skull of *Diplometopon zarudnyi*: (1) shortening the skull to increase its efficiency as a penetrating tip for the ramming action during burrowing and (2) ensuring enough space for the sensory and nervous systems and other activities like feeding (Gans, 1960). An angle in the skull is a simple way of reducing the length of the skull while still maintaining functional length for those systems and activities (Gans, 1960). The angle has effects beyond this compromise as well. First, the angle alters how burrowing forces are transmitted throughout the skull because they no longer are transmitted along a longitudinal axis but at an angle instead (Gans, 1960). Head angle has been shown to affect skull stress during burrowing in caecilians (Kleinteich et al., 2012), so there is likely an optimal angle for burrowing in *Diplometopon zarudnyi* as well. The angle also helps

protect the mouth during burrowing by deflecting the tooth row away from the tip of the rostrum (Gans, 1960). Therefore, variation in the angle of the rostrum can affect the biomechanics of the skull of *Diplometopon zarudnyi* in many ways. That variation may even influence other areas of variation like the frontal-parietal interdigitation because the transmission of burrowing forces is involved in both regions.

4.2.4 | Sagittal crest

The sagittal crest is well known to vary with ontogeny in other taxa, so it is no surprise to find the same result in *Diplometopon zarudnyi*. The sagittal crest serves as an attachment site for the external jaw adductor muscles (Rieppel, 1979). In *Amphisbaena*, the allometric growth of those muscles results in ontogenetic change to the amphisbaenian skull, including lengthening and solidifying of the sagittal crest (Gans & Alexander, 1962; Gans & Montero, 2008). In *Diplometopon zarudnyi*, ontogenetic variation in the sagittal crest is supported by the positive, significant correlation between snout-vent length and parietal PC 1 (representing the strength of the sagittal crest and projection of the otic-occipital lappet). The same caveats for the other correlations still apply to this finding, including the fact that the correlation between maximum skull length and parietal PC 1 is positive but not significant. But, because ontogenetic variation in the sagittal crest is well established in amphisbaenians and other taxa, there is still validity to this finding.

4.3 | Study limitations

The greatest limitations of our study are the relatively low number of specimens, specimen preservation, and lack of data on locality, age, sex, and body measurements (when fresh). Our sample of seven individuals permitted a preliminary examination of intraspecific variation, but our sample does not capture the full range of variation possible within *Diplometopon zarudnyi* as evidenced by other authors observing states not observed in our sample. Additionally, because the specimens lack certain data, we were unable to correlate our results with attributes like biogeography, habitat, and sex. The specimens were also desiccated, making their snout-vent length and total length measurements potentially inaccurate compared to living specimens. As such, we consider our results to be a preliminary assessment of the range of intraspecific variation expressed in *Diplometopon zarudnyi*.

5 | CONCLUSIONS

Intraspecific variation has not been emphasized in studies of the osteology of amphisbaenians, but it is important for understanding the range of morphologies possible within a species and across the broader clade to which that species belongs, especially in regard to biomechanical, ontogenetic, and environmental influences. Here, we examined intraspecific variation in the amphisbaenian *Diplometopon zarudnyi*. Our findings show variation in the number and placement of foramina, pattern of frontal-parietal interdigitation, extent of coossification of the occipital region, angle of the rostrum, and shape of various skull elements. Additionally, we revealed a potential post-natal ontogenetic coossification sequence and new fusion state for the occipital region. The patterns of variation that we observed could be tied to biomechanics, ontogeny, and/or random variation around a minimally adequate skull configuration that permits survival under the pressures and constraints of the burrowing habits of the species.

Further research is needed to determine the relative importance of these and other extrinsic and intrinsic factors in intraspecific variation in *Diplometopon zarudnyi*. For example, intraspecific variation could be examined in specimens of known ages from across the ontogenetic sequence to test for an ontogenetic influence, or finite element analysis could be used to test the biomechanical implications of the morphological variations reported here. Overall, our findings may be applicable not only to other amphisbaenians, but to other HFB taxa like other squamates and caecilians because members of those taxa experience similar selective pressures on their cranial morphology.

AUTHOR CONTRIBUTIONS

Rebecca K. Hawkins: data curation; formal analysis; investigation; methodology; software; validation; visualization; writing—original draft preparation; writing—review and editing. **Christopher J. Bell**: investigation; validation; writing—review and editing. **Jennifer C. Olori**: funding acquisition; investigation; validation; writing—review and editing. **Michelle R. Stocker**: conceptualization; funding acquisition; investigation; methodology; project administration; resources; supervision; validation; writing—review and editing.

ACKNOWLEDGMENTS

This work was supported by the National Science Foundation (NSF) award number 1655609 to Michelle R. Stocker and Jennifer C. Olori. We are grateful to the late Dr. Carl Gans for providing the specimens of *Diplometopon zarudnyi*, Dr. Jessica Maisano from the High-Resolution X-ray Computed Tomography Facility at The University of Texas at Austin (UTCT) for microCT-scanning the specimens, Krista Koeller and George Gurgis for guidance on the geometric morphometric analyses, and Brenen Wynd for guidance on statistics and figure design.

CONFLICT OF INTEREST

The authors declare no conflict of interest.

DATA AVAILABILITY STATEMENT

All CT scans and skull 3D models are uploaded and freely available for download at MorphoSource under the project "Diplometopon zarudnyi" (https://www.morphosource.org/projects/000369111).

ORCID

Rebecca K. Hawkins http://orcid.org/0000-0002-1110-8872

REFERENCES

Abo-Eleneen, R. E., Othman, S. I., Al-Harbi, H. M., Abdeen, A. M., & Allam, A. A. (2019). Anatomical study of the skull of amphisbaenian *Diplometopon zarudnyi* (Squamata, Amphisbaenia). *Saudi Journal of Biological Science*, *26*(3), 505–513. https://doi.org/10.1016/j.sjbs.2017.07.011

Adams, D. C., & Otárola-Castillo, E. (2013). Geomorph: An R package for the collection and analysis of geometric morphometric shape data. *Methods in Ecology and Evolution*, *4*, 393–399. https://doi.org/10.1111/2041-210X.12035

Al-Hassawi, A. M. A. (2004). *The osteology and myology of the craniocervical region in squamate reptiles: A comparative study* (Publication No. PQ ETD:602430) [Doctoral dissertation, University College London]. UCL Discovery.

Al-Sadoon, M. K., Paray, B. A., & Rudayni, H. A. (2016). Diet of the worm lizard, *Diplometopon zarudnyi* (Nikolsky, 1907), in Riyadh Province, Saudi Arabia (Reptilia: Trogonophidae). *Zoology in the Middle East*, *62*(3), 227–230. https://doi.org/10.1080/09397140.2016.1226243

Behbehani, S. J. Y., Els, J., Soorae, P., Al Johany, A. M. H., & Papenfuss, T. (2012). *Diplometopon zarudnyi*. The IUCN Red List of Threatened Species. Retrieved November 13, 2020 from https://www.iucnredlist.org/species/164643/1063445

Boyer, D. M., Puente, J., Gladman, J. T., Glynn, C., Mukherjee, S., Yapuncich, G. S., & Daubechies, I. (2015). A new fully automated approach for aligning and comparing shapes. *The Anatomical Record*, *298*, 249–276. https://doi.org/10.1002/ar.23084

Conith, A. J., Lam, D. T., & Albertson, R. C. (2019). Muscle-induced loading as an important source of variation in craniofacial skeletal shape. *Genesis*, *57*(1), e23263. https://doi.org/10.1002/dvg.23263

Curtis, N., Jones, M. E. H., Evans, S. E., O'Higgins, P., & Fagan, M. J. (2013). Cranial sutures work collectively to distribute strain throughout the reptile skull. *Journal of the Royal Society Interface*, *10*(86), 20130442. https://doi.org/10.1098/rsif.2013.0442

El-Assy, Y. S., & Al-Nassar, N. A. (1976). Morphological study of the cranial osteology of the amphisbaenian *Diplometopon zarudnyi*. *Journal of the University of Kuwait (Science)*, *3*, 113–141.

Gans, C. (1960). Studies on amphisbaenids (Amphisbaenia, Reptilia) 1. A taxonomic revision of the Trogonophinae and a functional interpretation of the amphisbaenid adaptive pattern. *Bulletin of the American Museum of Natural History*, *119*, 129–204.

Gans, C. (1974). *Biomechanics: An approach to vertebrate biology*. J. B. Lippincott Company.

Gans, C. (1978). The characteristics and affinities of the Amphisbaenia. *The Transactions of the Zoological Society of London*, *34*(4), 347–416. https://doi.org/10.1111/j.1096-3642.1978.tb00376.x

Gans, C. (1993). On the merits of adequacy. *American Journal of Science*, *293(A)*, 391–406. https://doi.org/10.2475/ajs.293.A.391

Gans, C. (2005). Checklist and bibliography of the Amphisbaenia of the world. *Bulletin of the American Museum of Natural History*, *289*, 1–130. https://doi.org/10.1206/0003-0090(2005)289<0001:CABOTA>2.0.CO;2

Gans, C., & Alexander, A. A. (1962). Studies on amphisbaenids (Amphisbaenia, Reptilia) 2. On the amphisbaenids of the Antilles. *Bulletin of the Museum of Comparative Zoology at Harvard College*, *128*, 65–158.

Gans, C., & Montero, R. (2008). An atlas of amphisbaenian skull anatomy. In Gans, C., Gaunt, A. S. & Adler, K. (Eds), *Biology of the Reptilia, vol. 21, Morphology I: The skull and appendicular locomotor apparatus of Lepidosauria* (pp. 621–738). Society for the Study of Amphibians & Reptiles.

Gauthier, J. A., Kearney, M., Rieppel, O., Maisano, J. A., & Behlke, A. D. B. (2012). Assembling the squamate tree of life: Perspectives from the phenotype and the fossil record. *Bulletin of the Peabody Museum of Natural History*, *53*(1), 3–308. https://doi.org/10.3374/014.053.0101

Goetz, M. (2007). On the husbandry and reproduction of *Blanus cinereus* (Vandelli, 1797) (Squamata: Amphisbaenia) in captivity. *Salamandra*, *43*(1), 52–56.

Gower, J. C. (1975). Generalized procrustes analysis. *Psychometrika*, *40*, 33–51. https://doi.org/10.1007/BF02291478

Griffin, C. T., Stocker, M. R., Colleary, C., Stefanic, C. M., Lessner, E. J., Riegler, M., Formoso, K., Koeller, K., & Nesbitt, S. J. (2020). Assessing ontogenetic maturity in extinct saurian reptiles. *Biological Reviews*, *96*, 470–525. https://doi.org/10.1111/brv.12666

Herrel, A., Choi, H. F., Dumont, E., de Schepper, N., Vanhooydonck, B., Aerts, P., & Adriaens, D. (2011). Burrowing and subsurface locomotion in anguilliform fish: Behavioral specializations and mechanical constraints. *Journal of Experimental Biology*, *214*, 1379–1385. https://doi.org/10.1242/jeb.051185

Hipsley, C. A., Rentinck, M.-N., Rödel, M.-O., & Müller, J. (2016). Ontogenetic allometry constrains cranial shape of the head-first burrowing worm lizard *Cynisca leucura* (Squamata: Amphisbaenidae). *Journal of Morphology*, *277*, 1159–1167. https://doi.org/10.1002/jmor.20564

Kearney, M. (2003). Systematics of the Amphisbaenia based on morphological evidence from recent and fossil forms. *Herpetological Monographs*, *17*, 1–74. https://doi.org/10.1655/0733-1347(2003)017[0001:SOTALB]2.0.CO;2

Kearney, M., & Stuart, B. L. (2004). Repeated evolution of limblessness and digging heads in worm lizards revealed by DNA from old bones. *Proceedings of the Royal Society B*, *271*, 1677–1683. https://doi.org/10.1098/rspb.2004.2771

Kleinteich, T., Maddin, H. C., Herzen, J., Beckmann, F., & Summers, A. P. (2012). Is solid always best? Cranial performance in solid and fenestrated caecilian skulls. *Journal of Experimental Biology*, *215*(5), 833–844. https://doi.org/10.1242/jeb.065979

Lee, M. S. Y. (1998). Convergent evolution and character correlation in burrowing reptiles: Towards a resolution of squamate relationships. *Biological Journal of the Linnean Society*, *65*, 369–453. https://doi.org/10.1111/j.1095-8312.1998.tb01148.x

Longrich, N. R., Vinther, J., Pyron, R. A., Pisani, D., & Gauthier, J. A. (2015). Biogeography of worm lizards (Amphisbaenia) driven by end-Cretaceous mass extinction. *Proceedings of the Royal Society B*, *282*(1806), 20143034. https://doi.org/10.1098/rspb.2014.3034

Maisano, J. A. (2002). Postnatal skeletal ontogeny in *Callisaurus draconoides* and *Uta stansburiana* (Iguania: Phrynosomatidae). *Journal of Morphology*, *251*, 114–139. https://doi.org/10.1002/jmor.1078

Maisano, J. A., Kearney, M., & Rowe, T. (2006). Cranial anatomy of the spade-headed amphisbaenian *Diplometopon zarudnyi* (Squamata, Amphisbaenia) based on high-resolution X-ray computed tomography. *Journal of Morphology*, *267*, 70–102. https://doi.org/10.1002/jmor.10388

Moazen, M., Curtis, N., O'Higgins, P., Jones, M. E. H., Evans, S. E., & Fagan, M. J. (2009). Assessment of the role of sutures in a lizard skull: A computer modelling study. *Proceedings of the Royal Society B: Biological Sciences*, *276*(1654), 39–46. https://doi.org/10.1098/rspb.2008.0863

Montero, R., Daza, J. D., Bauer, A. M., & Abdala, V. (2017). How common are cranial sesamoids among squamates? *Journal of Morphology*, *278*(10), 1400–1411. https://doi.org/10.1002/jmor.20719

Preuschoft, H., & Witzel, U. (2002). Biomechanical investigations on the skulls of reptiles and mammals. *Senckenbergiana lethaea*, *82*, 207–222. https://doi.org/10.1007/BF03043785

Pyron, R. A., Burbrink, F. T., & Wiens, J. J. (2013). A phylogeny and revised classification of Squamata, including 4161 species of lizards and snakes. *BMC Evolutionary Biology*, *13*. https://doi.org/10.1186/1471-2148-13-93

Rieppel, O. (1979). The external jaw adductor of amphisbaenids (Reptilia: Amphisbaenia. *Revue Suisse de Zoologie*, *86*, 867–876. https://doi.org/10.5962/bhl.part.82344

Rudayni, H. A., Al-Sadoon, M. K., & Paray, B. A. (2017). Morphological characteristics of worm lizard, *Diplometopon zarudnyi* (Squamata: Trogonophidae), in the central region of Saudi Arabia. *Saudi Journal of Biological Science*, *24*, 966–971. https://doi.org/10.1016/j.sjbs.2016.12.003

Sherratt, E., Gower, D. J., Klingenberg, C. P., & Wilkinson, M. (2014). Evolution of cranial shape in caecilians (Amphibia: Gymnophiona. *Evolutionary Biology*, *41*, 528–545. https://doi.org/10.1007/s11692-014-9287-2

Da Silva, F. O., Fabre, A.-C., Savriama, Y., Ollonen, J., Mahlow, K., Herre, A., Müller, J., & Di-Poï, N. (2018). The ecological origins of snakes as revealed by skull evolution. *Nature Communications*, *9*(376), 376. https://doi.org/10.1038/s41467-017-02788-3

How to cite this article: Hawkins, R. K., Bell, C. J., Olori, J. C., & Stocker, M. R. (2022). Intraspecific variation in the cranial osteology of *Diplometopon zarudnyi* (squamata: Amphisbaenia: Trogonophidae). *Journal of Morphology*, *283*, 1359–1375. https://doi.org/10.1002/jmor.21508